Robust and efficient algorithms for rapid prototyping of heterogeneous objects

X.Y. Kou and S.T. Tan
Department of Mechanical Engineering, The University of Hong Kong, Hong Kong

Abstract

Purpose – Apart from the geometries to be dealt with, rapid prototyping (RP) of heterogeneous objects requires additional material information to be processed. This generally involves a large amount of information to be processed simultaneously. The robustness and efficiency problems, which seem less critical in homogeneous solid fabrications, become an issue. The direct impetus of this paper is to present robust and efficient algorithms for RP of heterogeneous objects.

Design/methodology/approach – The robustness is benefited from using the proposed non-manifold heterogeneous cellular model, which guarantees gap-free material depositions around material interfaces. The efficiency enhancement is achieved by eliminating repetitive boundary intersections and using a heuristic material interrogation approach.

Findings – By using the proposed algorithms, the robustness and efficiency of RP of heterogeneous objects can be improved. It is found that an average 30 percent efficiency improvement is obtained using the proposed heuristic material interrogation approach.

Originality/value – Non-manifold heterogeneous cell representation (HC-Rep) is used in RP fields for the first time. Based on the HC-Rep, the robustness and efficiency of RP of heterogeneous object is addressed in this paper.

Keywords Rapid prototypes, Composite materials, Physical properties of materials

Paper type Research paper

Introduction

The term "heterogeneous objects" generally refer to objects made of different constituent materials or spatially different structures (Kou and Tan, 2007a). The need for utilizing heterogeneous objects stems from the fact that the users' functional requirements are usually multiple and conflicting, and can hardly be fulfilled by a single homogeneous material. For instance, few materials can simultaneously render high hardness and toughness, good stress shielding and biocompatibility, sufficient mechanical strength and heat resistance, etc.

By using multiple materials and properly tailoring the material heterogeneities, however, the user's multifold (sometimes contradictory) requirements can be satisfied. For instance, modern space shuttles are subjected to high temperatures (over 1,400°C; Musikant, 1991) and enormous loads. In terms of thermal resistance, ceramics are good candidate materials because of their high heat capacity and excellent corrosion resistance; however they cannot sustain strong forces. Conversely, aluminum has good strength and toughness but they fail to survive under severe temperatures (the melting point of aluminum is 660°C). A solution to surmount this is to utilize metal substrates as the skeletons and ceramic materials as coatings. Gradual material transitions from pure metals to pure ceramics can be utilized to alleviate the delamination problem due to the thermal expansion mismatch of ceramics and metals (Cooley, 2005), as shown in Figure 1.

Because of many such favorable properties and unique features, *modeling* (CAD) (Adzhiev *et al.*, 2002; Bhashyam *et al.*, 2000; Biswas *et al.*, 2004; Kou and Tan, 2005; Kou *et al.*, 2006; Kumar and Dutta, 1998; Liu *et al.*, 2004; Qian and Dutta, 2003a; Xu and Shaw, 2005), *analysis* (CAE) (Kou and Tan, 2007b; Elishakoff *et al.*, 2005; Cho and Ha, 2002; Praveen and Reddy, 1998; Nemat-Alla, 2003), and *fabrication* (CAM) of heterogeneous objects have gained significant research focus in recent years.

With the recent development in solid freeform fabrication technologies, rapid prototyping (RP) methods have shown to be effective approaches for the physical realization of heterogeneous objects. Considerable research efforts (Cho *et al.*, 2002; Khalil *et al.*, 2004; Zhou, 2004a,b; Kou and Tan, 2006; Hu *et al.*, 2005; Zhou *et al.*, 2004; Tandon and Kant, 2004) have been made in the RP communities and systematic solutions are investigated. Nevertheless, many of the existing methods simply apply traditional models and algorithms which are well suited for homogeneous solid fabrications (for instance, assembly models are used to represent and fabricate multi-material objects); however significant robustness and efficiency problems arise (see the next section for details). The direct impetus of this paper is to present robust and efficient algorithms for RP of heterogeneous objects, particularly those with complex material heterogeneities. The robustness is benefited from using the proposed non-manifold heterogeneous cellular model, which warrants gap-free material depositions around

The current issue and full text archive of this journal is available at
www.emeraldinsight.com/1355-2546.htm

Rapid Prototyping Journal
15/1 (2009) 5–18
 [ISSN 1355-2546]
[DOI 10.1108/13552540910925018]

Received: 27 April 2007
Revised: 6 August 2007
Accepted: 5 February 2008

Figure 1 Heterogeneous material distribution examples

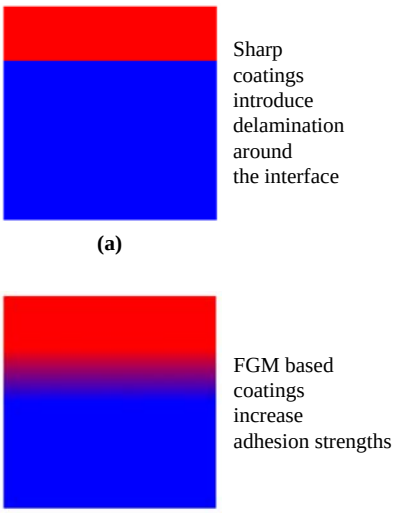

Notes: (a) A multi-material distribution; (b) A Functionally Graded Material (FGM) distribution. Red and blue colours are used to represent the pure ceramic and metal materials; the blended colors represent the graded materials

material interfaces. The efficiency enhancement is achieved by eliminating repetitive boundary intersections and using a heuristic material interrogation approach.

The remainder of this paper is logically organized as follows. Related work and the motivations of this paper are first described. The proposed data structures and algorithms are then presented; implementation details and application examples of the proposed algorithms are offered. Finally, conclusions are drawn and discussions are provided.

Previous work and motivations

Basic algorithms for rapid prototyping of homogeneous solids

A typical flow path in RP of a *homogeneous* solid can be roughly described as follows:

- With a given build direction, the object geometry is first sliced by an array of parallel planes and the sectioned boundary profiles are obtained, as shown in Figure 2(a) and (b).
- For each slice, the silhouette boundary curves (Weiss *et al.*, 1997) are covered into an array of 2D regions (in Figure 2(c), two regions are covered).
- Intersect each 2D region with parallel scan lines and get a collection of 1D intervals where materials are to be deposited/solidified.
- Use the obtained data to drive the hardware setup (e.g. nozzles, lasers, etc.) to deposit/solidify materials in a voxel-wise, line-wise, and slice-wise fashion until the whole object has been thoroughly fabricated, as shown in Figure 2(d).

Rapid prototyping of heterogeneous object

Heterogeneous objects are generally characterized as having local material compositions (Liu *et al.*, 2004; Cho *et al.*, 2003; Jackson *et al.*, 1999). In the context of layered manufacturing

Figure 2 A typical flow path in RP of a homogeneous object

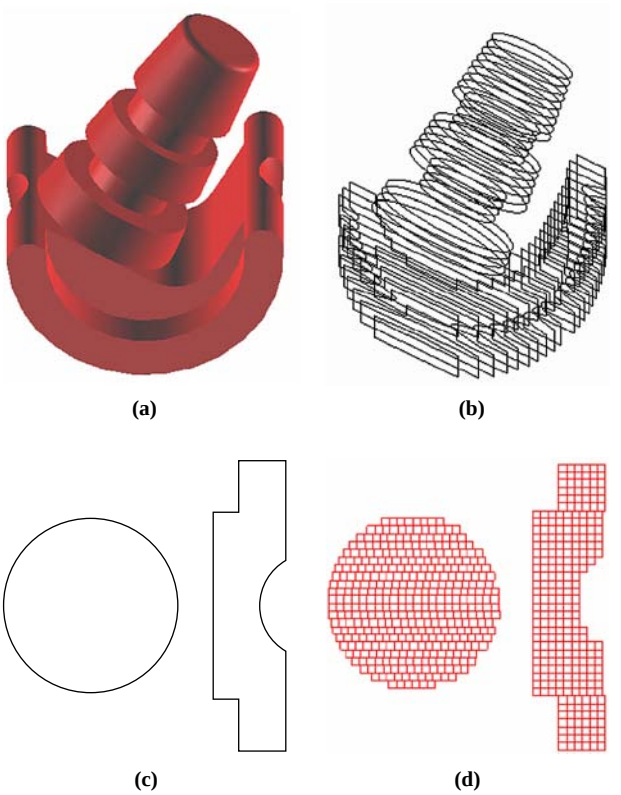

Notes: (a) Input 3D homogeneous solid; (b) Sliced boundary curves; (c) One of the selected slices; (d) Voxelized 2D slice of the 2D region

of heterogeneous objects, location dependent material data should be incorporated so that different materials can be selectively deposited/solidified at each voxel/lump (Vijay *et al.*, 1995).

To facilitate RP of functionally graded material (FGM) objects, Siu and Tan (2002) and Zhou *et al.* (2004) introduced the material grading references to represent *unidirectionally* graded distributions. The distance from the point of interest to the reference features are regarded as the material variation variables; explicit, analytic functions were used to evaluate the local material compositions. Kou and Tan (2005) proposed a hierarchical representation to model heterogeneous objects with compound (*bidirectional* or *trivariate*) material distributions: the geometry and topology were represented with the well established B-Rep model and the material distribution was represented with "heterogeneous feature tree" (HFT) structures. To get the necessary material information required in the RP process, a recursive material evaluation algorithm was proposed (Kou and Tan, 2005; Kou, 2006). Qian and Dutta (2003a), Hua *et al.* (2004), and Martin and Cohen (2001) also proposed B-spine tensor product models to represent heterogeneous objects with *trivariate* material distributions.

Once these heterogeneous CAD models (Kou and Tan, 2007a) are constructed, the planar slicing, region covering and line scanning processes discussed in previous subsection can be similarly executed. Each voxel's material is then retrieved from the CAD model and the material with interrogated composition is deposited and solidified at each voxel, as illustrated in Figure 3.

Figure 3 RP of a heterogeneous object

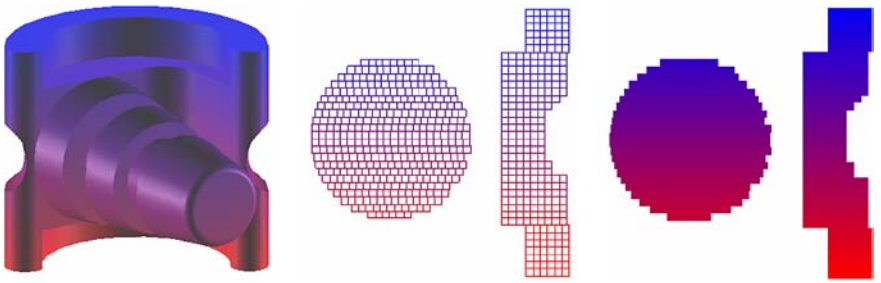

(a) **(b)** **(c)**

Notes: (a) A unidirectional FGM object; (b) A voxelized 2D slice of (a); (c) A shaded visualization of (b)

Challenges and motivations

From Figures 2 and 3, it appears that if the local material compositions can be properly evaluated or interrogated, existing algorithms for RP of *homogeneous* solids can be almost completely immigrated to the *heterogeneous* object fabrications; there is no apparent significance to explicitly distinguish these two. Indeed, such an assertion is true if the objects of interest always have *simple* and *regular* material distributions as illustrated above. Here, we regard such material distributions as *simple* because throughout the objects' geometries, the material distribution is formulated with a *single* material mapping function (Kou and Tan, 2007a), no matter if it is 1D (Siu and Tan, 2002), 2D (Kou and Tan, 2005) or 3D (Qian and Dutta, 2003a) dependent on the spatial locations. More intuitively, simple material distribution can be either homogeneous, 1D or 2D graded, but not the hybrids. For general heterogeneous objects, however, it is possible that more than one generically different material distributions coexist in different portions (sub-domains) of the object (Kou and Tan, 2007a; Kou *et al.*, 2006; Cheng and Lin, 2005; Shin, 2002; Chen and Tucker, 2000). In the scenarios where the objects under fabrication have complex material heterogeneities, simply applying the above discussed algorithms may result in significant robustness and efficiency problems.

Consider the layered manufacturing of the heterogeneous object shown in Figure 4 as an example. This object is composed of five components: three homogeneous objects O_1, O_3, O_5 and two FGM component O_2 and O_4 (Figure 4(b)). An intuitive and widely used approach is to represent the object with an assembly model. For instance, Langrana *et al.* (2000) and Weiss *et al.* (1997) used the assembly models (multiple standard template library (STL) files or multiple "nonlinear CAD models" (Weiss *et al.*, 1997) to represent *multi-material* objects, each of which represents a homogeneous component. The benefit of using the assembly model lies in its direct intuition and easy implementation; however, if the conventional part-assembly model (Figure 4(c)) is used, then the above *planar slicing* algorithm will be separately applied to each of the component, O_i ($i = 1,2,\ldots,5$), as illustrated in Figure 4(d).

Note that the face pairs (F_a, (F_a, F'_a)), (F_b, (F_b, F'_b)), (F_c, (F_c, F'_c)), etc. in Figure 4(c) represent exactly the same face geometry; however to get the boundary silhouette curves of each component, *identical* face-plane intersections must be *separately* applied on each face. This results in unnecessary and repetitive calculations. Similarly in the line scanning process, identical line-edge intersections will be conducted on the edges e_i and e'_i ($i = 1,2,\ldots,5$), which represent the same silhouette curve, as shown in Figure 4(d). As is seen from Figures 2 and 3 that the plane-face and line-edge intersections are intensively used in the RP process, therefore these repetitive boundary-intersection computations will dramatically degrade the computation efficiencies.

More importantly, the involved data redundancies also result in severe *data consistency* and *robustness* problems. It is well known that due to the finite hardware resolution, the staircase effect is commonplace around the object boundaries (i.e. start and end points of any scan lines). According to the algorithm presented above, the scan lines in $\overline{P_iP'_i}$ ($i = 1, 2, \ldots, 5$) Figure 5(a) will be independently decomposed into voxels (because these voxels are generated from separate parts); therefore the staircase effect occurs around all the points P_i and P'_i. Note that in homogeneous object fabrications, such stepping effect only influences the boundary qualities or geometric accuracies, however in RP of heterogeneous objects, these staircases occur in the *internal* portions of the objects, resulting in either material gaps/voids or superfluous/overlapping material depositions, as demonstrated in Figure 5(b) and (c). Such fabrication flaws may accumulate line by line and layer by layer, which significantly undermine the strength of the object and ultimately, result in fabrication failures.

It can be found out that the above efficiency and robustness problems are mainly provoked due to the existence of the redundant entities such as F_a, F'_a, e_i and e'_i, etc. It is evident that such entities serve as the delimitation boundaries of sub-domains which have different material distributions. They are introduced solely for the purpose of point containment test and material interrogations (Kou *et al.*, 2006; Qian and Dutta, 2003b). Conceptually, such material delimitation entities should not be included in the irrelevant geometric operations (such as section slicing and line scanning); instead, they should be utilized only in the material evaluation process.

Most of the existing approaches, however, either targeted for RP of objects with simple material distributions (Kou and Tan, 2006; Zhou *et al.*, 2004; Siu and Tan, 2002) or simply use the conventional models and algorithms (Langrana *et al.*, 2000) as mentioned earlier. The robustness and efficiency problems are seldom considered for objects with complex material heterogeneities. Weiss *et al.* (1997) first noted such data inconsistency problem and the possible effects of the "unpredictable and faulty" operations, however they solve the problems by manual checking to ensure reliable fabrications.

Figure 4 RP of an object with complex material heterogeneities

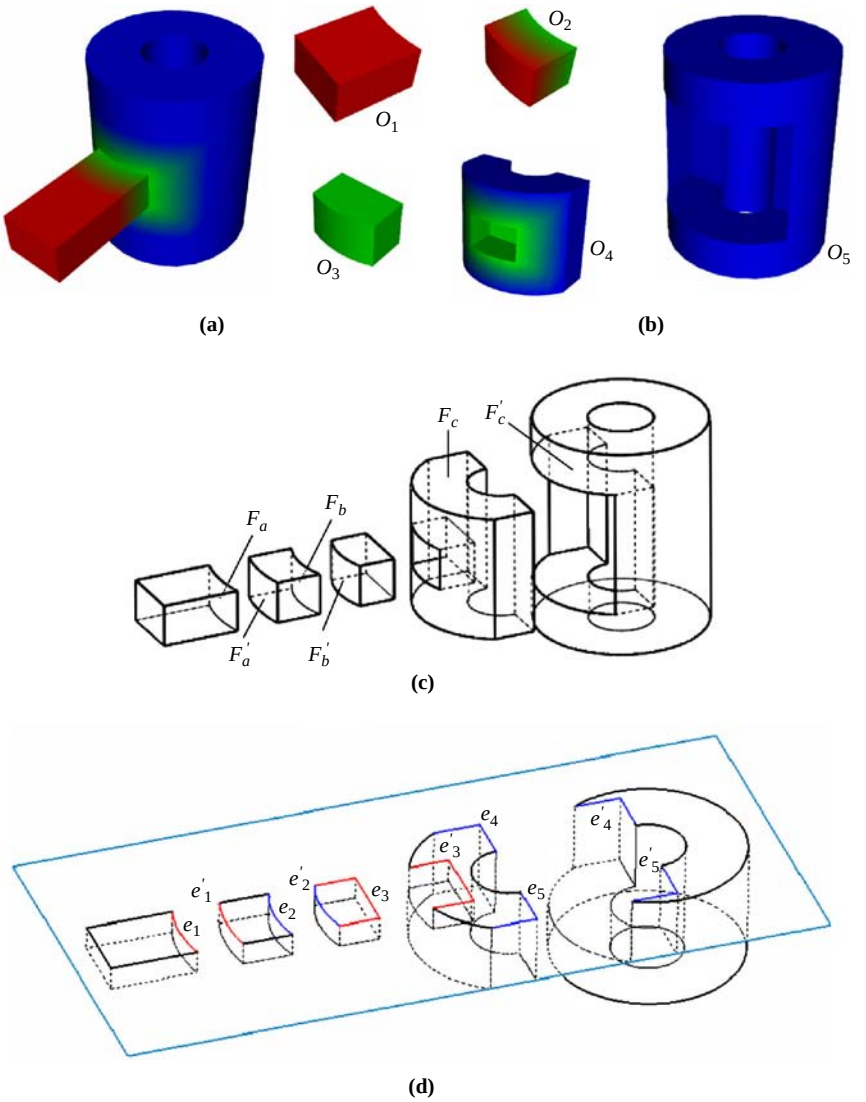

Notes: (a) 3D shaded view of the object; (b) Subdivided components of the object; (c) Assembly representation of the object geometries; (d) planar slicing of the assembly model

This paper provides an alternative approach to improving the robustness and efficiency of the RP of heterogeneous objects. The internal boundaries are automatically excluded from the boundary intersection and line scanning processes. A heuristic strategy is also proposed to speed up the material interrogations. The proposed methodologies are detailed as follows.

Robust and efficient algorithms for rapid prototyping of heterogeneous objects

Some assumptions

In what follows, we postulate that the build direction for the RP of a heterogeneous object is a fixed or a known parameter, since the proposed algorithms can be applied to circumstances with arbitrary build directions. Without loss of generality, the positive Z direction is assumed as the default build direction. The support material deposition, material affinity/compatibility and other problems, though equally important in practical RP fabrications, however are beyond the scope of this paper.

Heterogeneous cellular representation (HC-Rep)

To improve the robustness and efficiency, *irrelevant* boundary elements are temporarily excluded from the boundary intersection computations. Figure 6 demonstrates a desired planar slicing and line scanning configuration for the object shown in Figure 4(a). In the planar slicing process, only the boundary elements which bound the object geometries are considered as *relevant* candidates and they actually participate in the plane-face intersections; all the other internal material-delimitation boundaries are regarded as *irrelevant* entities in this stage.

To accomplish this, one needs to provide unambiguous guidelines to distinguish the *relevant* and *irrelevant* boundary elements. With the traditional part-assembly model, this is almost unattainable since all the boundary elements are

Figure 5 (a) A line scanning of the 2D section in Figure 4(d); (b) material gaps due to independent slicing and scanning and (c) superfluous material depositions due to independent slicing and scanning

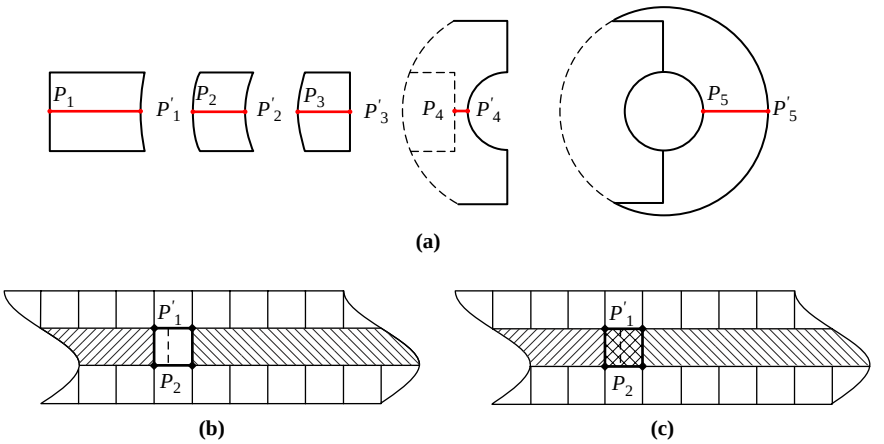

Notes: The regular box represents the fabrication resolution, and the dotted line represents the exact boundary position at P'_1 or P_2. The hatched regions represent the deposited materials

Figure 6 (a) Boundary intersection of a plane with relevant faces in planar slicing; (b) line scanning of the 2D region obtained in (a)

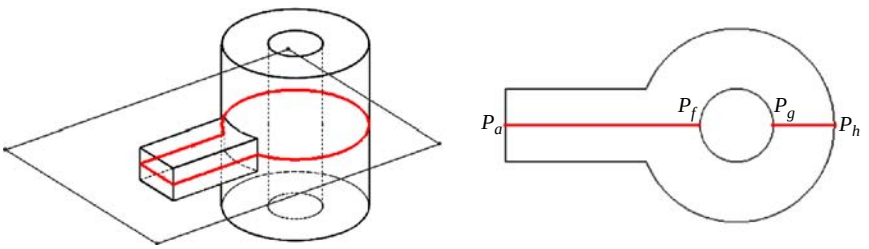

equally treated. In our previous paper (Kou *et al.*, 2006), we have proposed a heterogeneous cellular representation (HC-Rep) to represent objects with complex material heterogeneities and this HC-Rep model can be utilized to accomplish such a task. A complete description on the HC-Rep is out of the scope of this paper and interested reader may refer to Kou *et al.* (2006) and Kou (2006). For brevity and self-containedness, only the most relevant parts of HC-Rep are provided here.

The key idea of the HC-Rep is to combine the non-manifold cellular model (Bidarra *et al.*, 1998; Weiler, 1986; Keen, 1993) with the HFT structure (Kou and Tan, 2005; Kou, 2006) to represent heterogeneous objects. A heterogeneous object O is represented by *quasi-disjoint heterogeneous cells* (Kou *et al.*, 2006; Kou, 2006; Ferrucci, 1993). Contrary to the assembly model in which the material delimitation faces (e.g. F_a and F'_a in Figure 4(c)) are kept in separate part files, the HC-Rep maintains *only one copy* of such entities, as shown in Figure 7(b) and (d). Here, the cells O_1 and O_2 share the face F_a and cells O_2 and O_3 share the face F_b. These shared boundary elements are usually termed as co-boundaries. Due to the existence of such co-boundaries, the *manifold* conditions (i.e. "every point has a neighborhood which is *homeomorphic* to a two-dimensional disk" Weiler, 1988) are violated, resulting in the so-called *non-manifold* models (Keen, 1993). The non-manifold models can be constructed by applying the *non-regularized* (or *standard*) Boolean operations (Rossignac and Requicha, 1991).

To construct the cellular geometry in Figure 4(a), the following procedures are performed. A non-regular Boolean union is first applied on the input block B and cylinder C and the resultant object $U_1 = \{O_1, O_2, O_3\}$ is shown in Figure 7(b). Note that the internal boundaries F_a and F_b which delimit the sub geometric domains are kept in the resultant object, rather than obligated as is done with conventional *regularized* Boolean operators. After the first non-union Boolean union, the *connection cell* O_2 (Kou *et al.*, 2006) which corresponds to the mutual lump of B and C are identified. The connection cell is then offset by a user-input distance, as shown in Figure 7(c). The purpose of this offset is to offer a smooth material transition in between the input object B and C, as shown in Figure 4(b). The ultimate cellular geometry is then obtained by performing a second non-regular union of the offset object O_4 and U_1, as shown in Figure 7(d).

The material distributions of the non-manifold cells are modeled with the extended heterogeneous feature tree (eHFT) structures. The eHFT maintains the material variation dependencies among all the constructive heterogeneous features at different hierarchies. The material composition of a feature in a higher level is dependent on (or determined by) the material composition of its child features. By definition, the cells O_1, O_3, and O_5's material distributions (Figure 4(b)) are homogeneous (i.e. independent on other *heterogeneous features* Kou and Tan, 2005; Kou *et al.*, 2006; Kou, 2006), therefore their HFTs are represented with a NULL valued tree structure,

Figure 7 (a) Non-manifold cellular model construction process. (a) The input block B and cylinder C; (b) non-regular union B and C; (c) the offset of the *connection cell* (Kou *et al.*, 2006) and (d) the final cellular geometry obtained by applying non-regular union of the resultant object in (b) and (c)

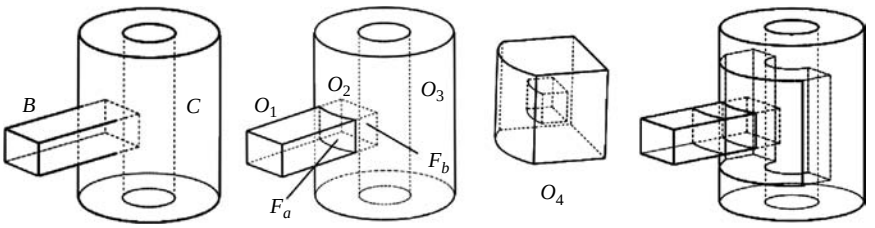

as demonstrated in Figure 8(a)-(c). The other two FGM cells O_2 and O_4 (Figure 4(b)) are represented with HFTs with two hierarchies: the parent level represents the cells O_2 and O_4's material distributions, the child levels are the feature nodes on which their material distributions depend, as conceptually demonstrated in Figure 8(d) and (e). Note that Figure 8 shows a simplified eHFT representation only and interested readers may refer to Kou *et al.* (2006) and Kou (2006) for the complete eHFT information and the detailed material modeling schemes.

Selective boundary slicing algorithm

By using the HC-Rep as described above, the unnecessary and repetitive boundary-interaction calculations can be avoided and this is accomplished by use of a selective boundary slicing algorithm.

Figure 8 The eHFT representations for the non-manifold heterogeneous cells

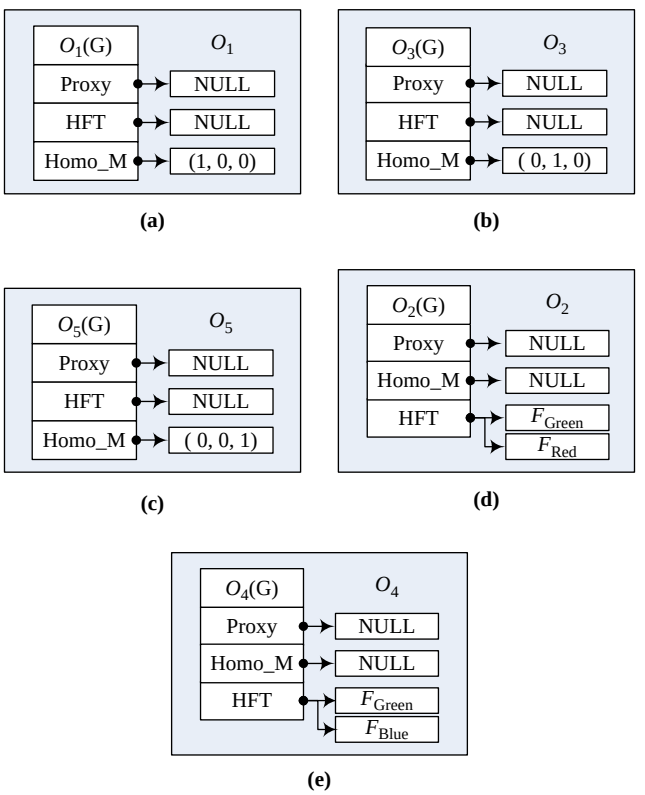

Notes: (a), (b), (c) are the eHFT representation for the homogeneous cells O_1, O_3 and O_5; (d) and (e) are the eHFT representation for the FGM O_2, O_4

As is seen from the comparison of Figures 6(a) and 7(d), the "irrelevant" entities in the boundary intersections are the internal material delimitation boundaries, which have the characteristics of sharing themselves with other boundary elements. These *irrelevant* entities, by definition, are nothing else but the co-boundaries described earlier. Such internal boundaries can be identified and then excluded from the planar slicing and line scanning computations. The pseudo code in Figure 9 describes the selective boundary slicing algorithm.

In this algorithm, all the boundary faces are first retrieved from the non-manifold cellular models (*L*8 in Figure 9); relevant faces to be used in the boundary intersection are then identified and saved in the "RelevantFaceList" (*L*11-*L*15). These faces are subsequently sewn together to form a manifold solid (*L*17) and other remaining faces are simply neglected. A further geometry simplification is carried out to remove unnecessary edges, and adjacent faces sharing such edges are merged wherever applicable (*L*19).

After applying the proposed algorithm on the discussed example, the original 41 faces (Figure 4(c)) in the part-assembly model are reduced to nine faces, and a 78 percent efficiency improvement is achieved in the plane-face intersections, as shown in Table I. Note that it is the boundaries of the *manifold* solid (Figure 10(a)) that participate in the actual planar slicing (*L*23) and region covering (*L*25), as shown in Figure 10(b).

Efficient material interrogations

Apart from the computation overhead in geometric operations (i.e. planar slicing, line scanning, and voxelization), the material composition evaluation in RP of heterogeneous object is also a time-consuming process. For a given voxel, a brute force algorithm might be sequentially applying the point membership classification (PMC) tests on all the candidate cells until the voxel is found to be on or inside a specific cell. Once the container cell (for instance O_1-O_5 in Figure 8) is obtained, the voxel's material composition can be then interrogated from the corresponding HFT structures. In the worst case, all the cells will be traversed, resulting in excessively long time in material interrogation.

In this section, we present a heuristic approach to infer the possible point containment status. The idea is based on the following observations:

- For each starting voxel in a scan line, there is no indicative information as to which cell the voxel belongs, a brute force PMC test should be conducted.

Figure 9 The pseudo code of the proposed selective boundary slicing algorithm

```
L 1   Input:  CSolid4D      *pInput;          The input object to be sliced (HC-Rep)
L 2   Output: CSectionArray *pOutputSlices;   The output sliced sections
L 3   SelectiveBoundary Slicing ( CSolid4D * pInput, CSectionArray*& pOutputSlices)
L 4   {
L 5       If ( IsNonManifold ( pInput-> GetGeometry( ) )
L 6       {
L 7           ENTITY_LIST AllFaces, RelevantFaceList, ManifoldGeometry;
L 8           api_get_faces_from_all_entities ( pInput, AllFaces );
L 9           foreach ( FACE* pFace in AllFaces )
L 10          {
L 11              if ( pFace ->sides ( ) = SINGLE_SIDED ) // Not a co-boundary element
L 12              {
L 13                  api_copy_entity_contents ( pFace, pFaceCopy );
L 14                  RelevantFaceList.add ( pFaceCopy );
L 15              }
L 16          }
L 17          api_stitch ( RelevantFaceList, ManifoldGeometry, ... );
L 18          BODY *pBodyTobeSliced = (BODY *) ManifoldGeometry[0];
L 19          api_clean_entity (pBodyTobeSliced);  //Clean unnecessary edges and associated data
L 20      }
L 21      for ( int i=0; i< nSections; i++)
L 22      {
L 23          api_planar_slice ( pBodyTobeSliced, ..., pSlicedWireBody );   //Planar slicing
L 24          ConvertWireBody2EntityList ( pSlicedWireBody, ProfileWireList );
L 25          api_cover_planar_wires ( ProfileWireList, p2DRegion, …);    //Region covering
L 26          pOutputSlices ->AddSectionGeometry(p2DRegion);
L 27      }
L 28  }
```

Note: The italic functions represent ACIS [45] APIs

Table I Number of faces involved in the plane-face intersections of different models

Models	Number of faces in the face-plane intersections
(a) Conventional assembly model	41
(b) The non-manifold cellular model	33
(c) After selective face exclusion of (b)	19
(d) After edge cleaning and face merging of (c)	9

Figure 10 The actual boundary elements used in the plane-face intersections and the slicing results

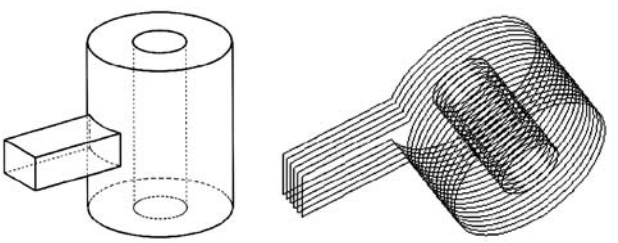

(a) **(b)**

Notes: (a) Relevant boundary elements derived by using the proposed algorithm; (b) The slicing result of applying the selective boundary slicing algorithm, a partial view

- If a voxel V_i is continuously deposited and inside the same cell C_{buffer} which contains the previously interrogated voxel V_{i-1}, then there is no need to perform the PMC test throughout the candidate cell list. Directly interrogate V_i's material composition in C_{buffer} will do. For instance, all the voxels along the scan line $\overline{P_{S1}P_1}$ and $\overline{P_{S2}P_{E2}}$ are in the same cell (as indicated with the same color in Figure 11) and in these cases there is no need to perform the brute force PMC tests.
- If a voxel V_i is discontinuously deposited, i.e. there are holes/gaps between V_{i-1} and V_i (for instance, the voxels at P_{E1} and P_{S2} in Figure 11), then there is no guarantee that these two voxels will be in the same cell, a brute force PMC test should be applied.
- The continuous or discontinuous status of two voxels can be judged by their x (line scanning direction) coordinate discrepancies, if it is bigger than the voxel's resolution,

Figure 11 PMC test using the internal material delimitation boundaries

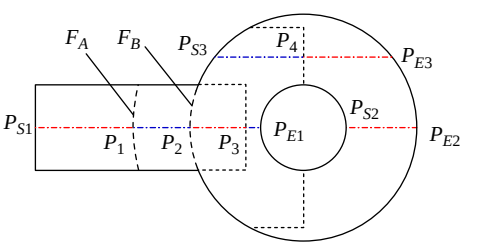

then these two voxels are discontinuously deposited (e.g. the voxels at P_{E1} andP_{S2}).

- To tell whether two voxels V_{i-1} and V_i are in the same cell, one can judge from their x (line scanning direction) coordinates. If V_i is located on the left side of the intersection point (e.g. P_1) of the scan line with the internal material delimitation boundary (e.g. F_A in Figure 11), then the current voxel V_i is in the same cell as V_{i-1}. Only when V_i's x coordinate is bigger than P_1's, do they fall inside different cells.
- The material delimitation points (e.g. P_1) can be obtained from the intersection of a ray (along the scan line direction) with the internal faces.

Based on the above observations, we can minimize the brute-force PMC tests through a heuristic approach. The pseudo code shown in Figure 12 describes the detailed algorithm.

In this algorithm, the cell which contains the last interrogated voxel V_{i-1} is explicitly kept in a buffer pBufferCell, see $L8$ in Figure 12. A scan line (e.g. the colored center line in Figure 13(a)) is first intersected with all the *internal* material delimitation boundaries (the black hidden lines in Figure 13(a)), see $L10$ in Figure 12 (note that the *internal* material delimitation boundaries can be identified with a similar algorithm as the one shown in Figure 9). All the x coordinates of the intersection points $P_{\text{int}} = \{P_1, P_2, P_3\}$ are then sorted in an ascending order and kept in a list KeyInterPos ($L11$ and $L13$).

For each voxel V_i under interrogation, we check if V_i is located on the left side of the head element of intersection points list P_{int} ($L21$). If the result is confirmative (for instance, the voxel V_1, V_{k-1}, and V_k in Figure 13(a) are on the left side of P_1), then it can be confirmed that the current voxel V_i and the previously interrogated voxel V_{i-1} are in the same

Figure 12 The pseudo code of an efficient material interrogation algorithm

```
L 1   Input:  CVoxel4DArray&  Voxels     The voxels in a scan line under material interrogation
L 2           CSolid4D        *pSolid;   The heterogeneous object of interest
L 3   Output: CVoxel4DArray&  Voxels     The voxels in the scan line, with material composition updated
L 4   HeuristicMaterialEvaluation (CVoxel4DArray& Voxels, CSolid4D* pSolid)
L 5   {
L 6       If ( IsNonManifold ( pSolid -> GetGeometry( ) )
L 7       {
L 8           CELL3D* pBufferCell = NULL;    //The cell container used in previous material evaluation
L 9           int nInternalFaces = pSolid -> Get_Internal_FaceList ( pInternalFaces );
L 10          api_ray_test_ents ( …, nInternalFaces, pInternalFaces, IntersectionPtList, …);
L 11          std::vector < double > KeyInterPos;
L 12          Get_X_Coords ( IntersectionPtList, KeyInterPos );
L 13          std::sort ( KeyInterPos.begin ( ), KeyInterPos.end ( ) );
L 14          for ( int i = 0; i < nVoxels; i++ )
L 15          {
L 16              if ( i != 0 )  //other than the first voxel in the scan line,
L 17              {
L 18                  double diff = Voxels[i]->X( )-Voxels[i-1]->X( );
L 19                  if ( diff <= 1.05*VoxelReso )   //Continuous voxels, 1.05 for robustness
L 20                  {     //Compare with the head of KeyInterPos, see if a key inter point is passed
L 21                      if ( !KeyInterPos.empty ( ) && Voxels[i]->X ( )->KeyInterPos.front ( ) )
L 22                      {
L 23                          KeyInterPos.erase ( KeyInterPos.begin ( ) );   //Update KeyInterPos
L 24                          pBufferCell = NULL;                            //Brute force PMC test;
L 25                      }
L 26                  }
L 27                  else pBufferCell = NULL; //Discontinuous, brute force PMC test
L 28                  pBufferCell = pSolid->EvalMaterial ( Voxels[i], pBufferCell );
L 29              }
L 30              else  //The first voxel in the scan line, brute force PMC test;
L 31                  pBufferCell = pSolid ->EvalMaterial ( Voxels[i], NULL );
L 32          }
L 33      }
L 34      else   //Manifold geometry, default PMC test.
L 35          for ( int i=0; i<nVoxels; i++ )      pSolid ->EvalMaterial ( Voxels[i], NULL );
L 36  }
```

Note: The italic function represents ACIS [45] APIs

Figure 13 A heuristic approach for efficient material interrogations

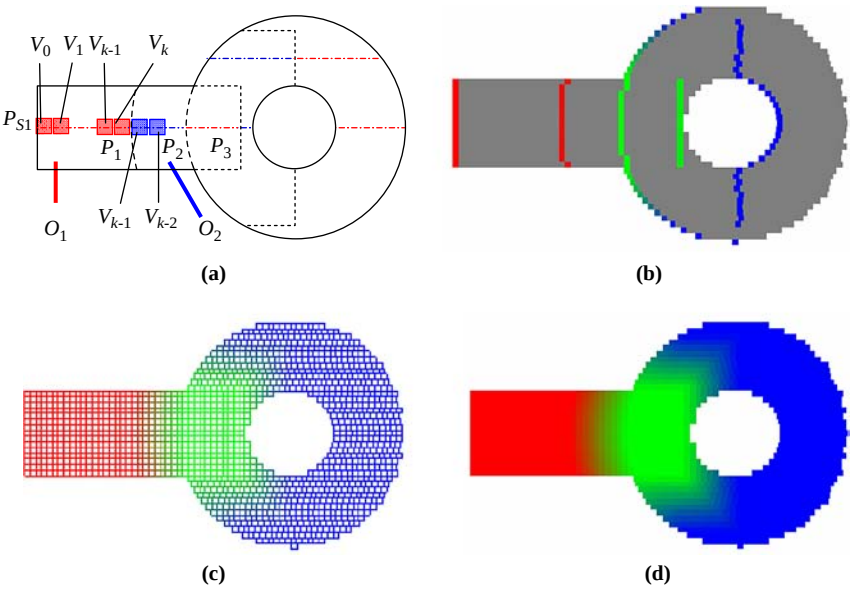

Notes: (a) Scan line subdivisions based on the internal material delimitation boundaries; (b) Voxels to be interrogated with the brute force PMC tests, highlighted with colors; grey voxel indicate voxels interrogated with the proposed heuristic approach; (c) Evaluated material compositions, a wire frame view; (d) Evaluated material compositions, a shaded view

heterogeneous cell, therefore there is no need to test V_i's containment throughout all the candidate cells. In this scenario, one can directly interrogate V_i's material composition from pBufferCell's HFT structure ($L28$), where the pBufferCell holds the cell which contains the previously interrogated voxel V_{i-1}. In the other case when V_i is located on the right side of the head element of P_{int} (for example, the voxel V_{k+1} in Figure 13(a) has gone across P_1), then voxel V_{k+1} and V_k are in different cells, a brute force PMC test needs to be applied on V_i ($L24$ and $L28$) to interrogate the voxel's containment; to implement this, pBufferCell is assigned a NULL pointer to indicate that no previous cells are available as the "shortcut" candidate containers. After the brute force PMC tests on V_{k+1}, the pBufferCell is updated with O_2 which contains the just interrogated voxel V_{k+1}, as shown in $L28$ in Figure 12 and Table II. Moreover, the KeyInterPos is also updated by removing the head element from the list ($L23$, Figure 12), for instance, P_1's x coordinate is removed and the intersection point list turns to be $P_{\text{int}} = \{P_2, P_3\}$ after V_{k+1} is traversed, as shown in Table II. For the next voxel along the scan line, which is V_{k+2}, the same check of its location with respect the head element of P_{int} (which is now P_2) is similar conducted, and the above heuristic PMC test continues.

By keep tracking of pBufferCell and the list KeyInterPos in such a manner, the brute force PMC tests are performed on limited voxels only, as highlighted with colored voxels in Figure 13(b). All the remaining voxels (grey colors in Figure 13(b)) are freed from the time-consuming PMC tests, and the materials are directly evaluated from pBufferCell's HFT structure. In the above discussed example, all the HFT structures are shown in Figure 8.

Table II The status of some key variables during the heuristic PMC tests

	pBufferCell		
Voxel under traversal	Before voxel traversal	After voxel traversal	P_{int} after voxel traveral
V_0	NULL	O_1	$P_{\text{int}} = \{P_1, P_2, P_3\}$
V_1	O_1	O_1	$P_{\text{int}} = \{P_1, P_2, P_3\}$
...	O_1	O_1	$P_{\text{int}} = \{P_1, P_2, P_3\}$
V_{k-1}	O_1	O_1	$P_{\text{int}} = \{P_1, P_2, P_3\}$
V_k	O_1	O_1	$P_{\text{int}} = \{P_1, P_2, P_3\}$
V_{k+1}	NULL	O_2	$P_{\text{int}} = \{P_2, P_3\}$
V_{k+2}	O_2	O_2	$P_{\text{int}} = \{P_2, P_3\}$

It should be noted that Figure 13(a) only demonstrated an ideal case where a voxel is precisely located on the left or right side of the intersection points P_i. Due to the finite voxel resolutions, it is common that the P_i falls within a voxel, as shown in Figure 14. Under such circumstances, we use the center location of the voxels to compare with the intersection point P_i. Depending on different material query strategies, such voxels' material composition may be evaluated from one of the HFT structures of the adjacent cells (e.g. O_1 and O_2 in Figure 14). Also note that such inexact material compositions only result in the so-called "material accuracy" (Kou, 2006) problems, however the materials are still consecutively deposited/solidified, and this is essentially different from the stair case effect depicted in Figure 5(b) and (c). As such, the proposed scheme can still ascertain the gap-free material

Figure 14 The material accuracy related to the voxel resolutions

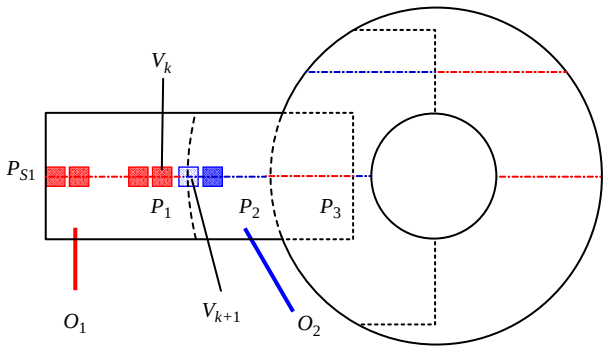

depositions in heterogeneous object fabrications and there is no strength loss arisen from the proposed algorithms.

The results of the proposed heuristic material evaluation algorithm are demonstrated in Figure 13(c), (d) and 15. Quantitative time consumptions of the brute force algorithm and the proposed heuristic approach are provided in Table III. For each fabrication resolution, three tests are conducted and the average time is used in evaluation of the efficiency improvement.

Implementations and examples

Implementations

The proposed algorithm has been successfully implemented in CAD4D (Kou and Tan, 2004) – a standalone heterogeneous object modeler developed by the authors at Department of Mechanical Engineering, The University of Hong Kong. CAD4D is based on the commercial geometric modeling kernel ACIS (www.spatial.com/products/acis.html) and the eHFT representations (Kou *et al.*, 2006; Kou, 2006). Microsoft foundation class libraries are utilized to implement the graphic user interface; C++ STL is used to implement container related data structures and algorithms; and OpenGL is used as the rendering engine for object visualizations.

A snapshot of CAD4D package is shown in Figure 16. Due to the literal inadequacy of a word written paper, we also provide three flash animations to demonstrate:

1 the HC-Rep model construction process;
2 application of the presented selective boundary intersection algorithm; and
3 application of the heuristic material evaluation algorithm.

These flash animations facilitate the readers to better understand the proposed scheme and are available for downloads at the authors' webpage http://web.hku.hk/~kouxy/CAD4D/CAM4D/.

Examples

In this section, we present several examples to demonstrate the application of the proposed scheme. Figure 17 shows the simulated RP of a heterogeneous propeller. The application of the selective boundary intersection algorithm is demonstrated in Figure 17(d), (g), and (j). The original 65 faces to be intersected (Figure 17(a)/(b)) are reduced to 14 faces after applying the proposed algorithm, and the 2D silhouettes (Figure 17(d), (g), and (j)) are therefore efficiently computed without unnecessary and repetitive plane-face intersections.

Figure 15 The material evaluation results for a heterogeneous layer under different resolutions

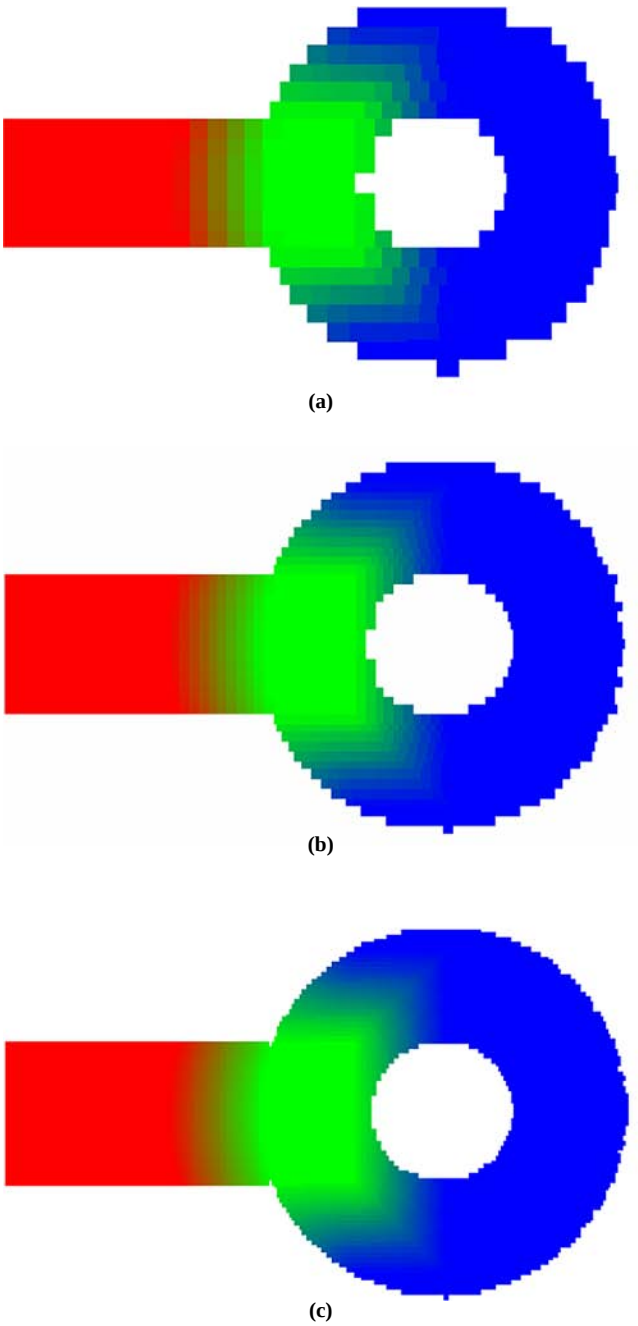

Notes: (a) a resolution of 2mm; (b) a resolution of 1mm; (c) a resolution of 0.5 mm

The evaluated material compositions of these 2D layers are shown in Figure 17(e), (f), (h), (i), (l), and (k). In the presented examples, an average 30 percent efficiency improvement is obtained using the proposed heuristic material interrogation approach.

To test and validate the proposed selective boundary intersection algorithm, we also fabricated a few prototypes using Z Corporation's 3D printer (www.zcorp.com/). The heterogeneous CAD models containing both the geometric

Table III Comparisons of the material evaluation time using the brute force and the proposed algorithm

Resolution	2 mm (Figure 13(a))			1 mm (Figure 13(b))			0.5 mm (Figure 13(c))		
Tests	*A*	*B*	*C*	*A*	*B*	*C*	*A*	*B*	*C*
Brute force algorithm (ms)	281	266	297	1,047	1,063	1,062	4,407	4,359	4,390
Improved algorithm (ms)	203	204	204	781	734	750	2,969	2,985	3,031
Average improvement (percent)		27.7			28.6			31.7	

Note: The results are tested on a desktop PC with 2.8 GHz CPU and 2G RAM

Figure 16 A snapshot of CAD4D graphic user interface

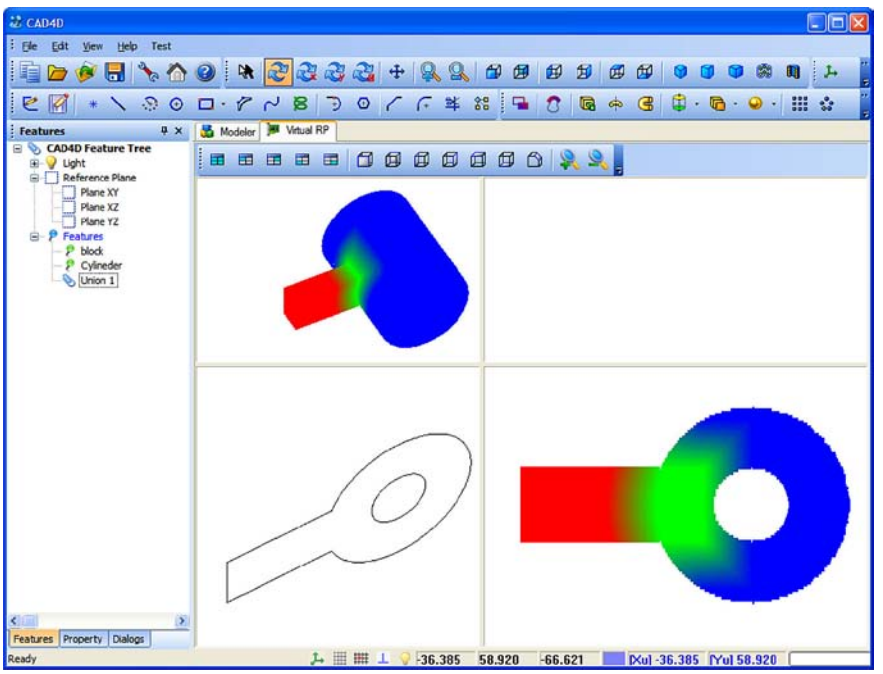

and material information are converted to VRML files with the CAD4D package. The generated VRML files contain only the boundary faces which are actually involved in the planar slicing processes. These VRML files are submitted to the 3D printer for physical fabrication. For the readers' interest, several such VRML files are also available for downloads in our web site. Some fabricated examples are shown in Figure 18(a) and (c). Notice that these prototypes show the object's external material distributions only. To demonstrate their internal material distributions, we also fabricated a few sliced prototypes, as shown in Figure 18(b) and (d).

Conclusions and discussions

RP of heterogeneous objects has received considerable research interest in recent years. Many existing methods simply reuse traditional solid models/algorithms and loosely attach the heterogeneous material distributions to the object geometries. At the cost of the legacy compatibility and easy implementation, significant robustness and efficiency problems arise.

This paper presents robust and efficient algorithms for RP of heterogeneous objects. A HC-Rep is used to model objects with complex material heterogeneities. Instead of simply using *all* the geometric boundaries in the planar slicing and material interrogation processes, the proposed scheme *selectively* choose the relevant entities in corresponding computations. A *selective* boundary intersection algorithm is proposed to eliminate repetitive boundary intersections. The efficiency of the planar slicing is significantly improved and gap-free material depositions around material interfaces are guaranteed. A heuristic material interrogation approach is also proposed to speed up the material evaluation process; brute force PMCs are carried out on limited voxels only. Software simulations and physical fabrication experiments show that the proposed approach can effectively improve the robustness and efficiency of RP of heterogeneous objects.

Due to the limited space, the construction of cellular geometric models is not fully elucidated as it involves the use of Radial-Edge structure (Weiler, 1988) and *non-regular* Boolean operations (Kou *et al.*, 2006; Rossignac and Requicha, 1991). Interested readers may find off-the-shelf implementations in the ACIS (www.spatial.com/components/) library. The complex heterogeneity modeling problem is not fully explained in this paper either, which is a new hotspot in heterogeneous object modeling and applications. The readers may refer to the recent review paper (Kou and Tan, 2007a) for more details on the existing modeling paradigms.

Figure 17 RP of a heterogeneous propeller using the proposed algorithm

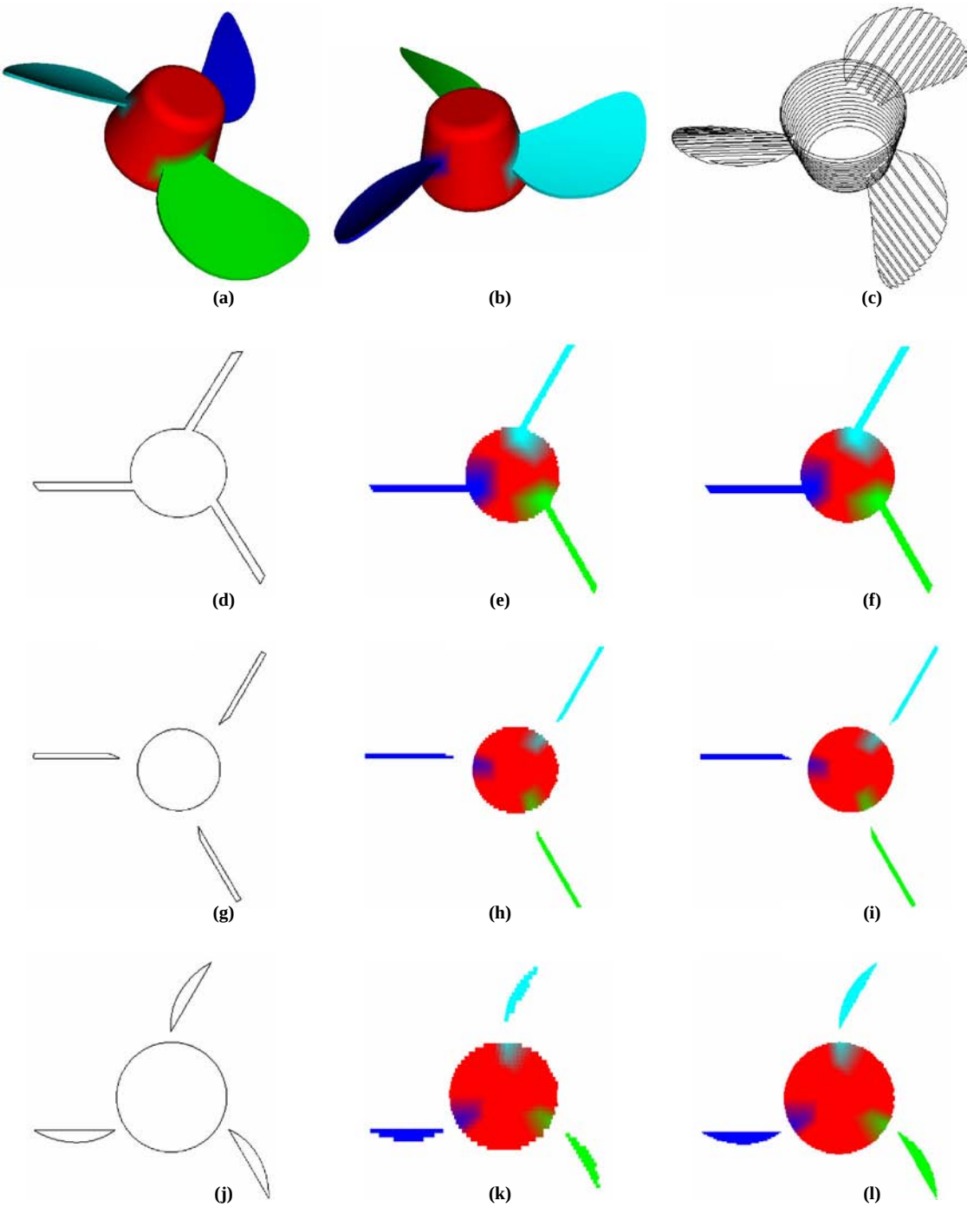

Notes: (a) and (b): 3D shaded view from two different perspectives; (c) Planar slicing using the proposed selective boundary intersection algorithm; (d), (g) and (j): example 2D slices; (e), (h) and (k): heterogeneous 2D layers rendered with a coarse resolution; (f), (i) and (l): heterogeneous 2D layers rendered with a fine resolution

Figure 18 Prototypes fabricated with 3D printer

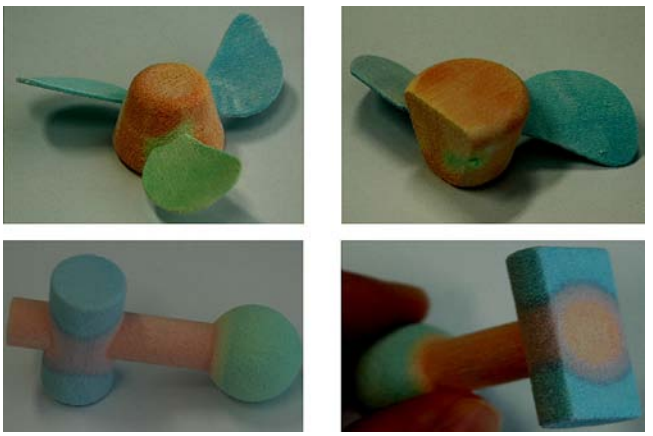

(a) **(b)**

Notes: (a) Complete prototypes; (b) Partial prototype showing the internal material distributions

References

Adzhiev, V., Kartasheva, E., Kunii, T., Pasko, A. and Schmitt, B. (2002), "Hybrid cellular-functional modeling of heterogeneous objects", *Journal of Computing and Information Science in Engineering*, Vol. 2, p. 312.

Bhashyam, S., Shin, K.H. and Dutta, D. (2000), "An integrated CAD system for design of heterogeneous objects", *Rapid Prototyping Journal*, Vol. 6, pp. 119-35.

Bidarra, R., de Kraker, K.J. and Bronsvoort, W.F. (1998), "Representation and management of feature information in a cellular model", *Computer-Aided Design*, Vol. 30, p. 301.

Biswas, A., Shapiro, V. and Tsukanov, I. (2004), "Heterogeneous material modeling with distance fields", *Computer Aided Geometric Design*, Vol. 21, pp. 215-42.

Chen, M. and Tucker, J.V. (2000), "Constructive volume geometry", *Computer Graphics Forum*, Vol. 19, pp. 281-93.

Cheng, J. and Lin, F. (2005), "Approach of heterogeneous bio-modeling based on material features", *Computer-Aided Design*, Vol. 37, p. 1115.

Cho, J.R. and Ha, D.Y. (2002), "Optimal tailoring of 2D volume-fraction distributions for heat-resisting functionally graded materials using FDM", *Computer Methods in Applied Mechanics and Engineering*, Vol. 191, pp. 3195-211.

Cho, W., Sachs, E.M., Patrikalakis, N.M. and Troxel, D.E. (2003), "A dithering algorithm for local composition control with three-dimensional printing", *CAD Computer Aided Design*, Vol. 35, pp. 851-67.

Cho, W., Sachs, E.M., Patrikalakis, N.M., Cima, M., Liu, H., Serdy, J. and Stratton, C.C. (2002), "Local composition control in solid freeform fabrication", *Proceedings of the NSF Design, Service and Manufacturing Grantees and Research Conference, San Juan, Puerto Rico.*

Cooley, W.G. (2005), "Application of functionally graded materials in aircraft structures", Master's thesis, Air Force Institute of Technology, Air University, Montgomery, AL.

Elishakoff, I., Gentilini, C. and Viola, E. (2005), "Three-dimensional analysis of an all-round clamped plate made of functionally graded materials", *Acta Mechanica*, Vol. 180, pp. 21-36.

Ferrucci, V. (1993), "Generalised extrusion of polyhedra", *Proceedings on the 2nd ACM Symposium on Solid Modeling and Applications, Montreal, Quebec, Canada*, p. 35.

Hu, Y., Blouin, V.Y. and Fadel, G.M. (2005), "Design for manufacturing of 3D heterogeneous objects with processing time consideration", *Proceedings of the ASME International Design Engineering Technical Conferences and Computers and Information in Engineering Conference – DETC2005, Long Beach, CA*, pp. 523-32.

Hua, J., He, Y. and Qin, H. (2004), "Multiresolution heterogeneous solid modeling and visualization using trivariate simplex splines", *Proceedings of the 9th ACM Symposium on Solid Modeling and Applications, Genova, Italy, June*, p. 47.

Jackson, T.R., Liu, H., Patrikalakis, N.M., Sachs, E.M. and Cima, M.J. (1999), "Modeling and designing functionally graded material components for fabrication with local composition control", *Materials and Design*, Vol. 20, pp. 63-75.

Keen, A.A. (1993), "A non-manifold shape representation", PhD thesis, Texas A&M University, College Station, TX.

Khalil, S., Nam, J., Darling, A. and Sun, W. (2004), "Multi-nozzle biopolymer deposition for freeform fabrication of tissue construct", *Proceedings of 15th Solid Freeform Fabrication Symposium, Austin, TX, USA, August 3-5.*

Kou, X.Y. (2006), "Computer-aided design of heterogeneous objects", PhD thesis, The University of Hong Kong, Hong Kong.

Kou, X.Y. and Tan, S.T. (2004), "An interactive CAD environment for heterogeneous object design", *Proceedings of ASME 2004 Design Engineering Technical Conferences, Salt Lake City, UT, USA, September 28-October 2.*

Kou, X.Y. and Tan, S.T. (2005), "A hierarchical representation for heterogeneous object modeling", *Computer-Aided Design*, Vol. 37, p. 307.

Kou, X.Y. and Tan, S.T. (2006), "Data structure and algorithms for virtual prototyping of heterogeneous objects", *Computer-Aided Design and Applications*, Vol. 3, pp. 59-67.

Kou, X.Y. and Tan, S.T. (2007a), "Heterogeneous object modeling: a review", *Computer-Aided Design*, Vol. 39, pp. 284-301.

Kou, X.Y. and Tan, S.T. (2007b), "A systematic approach for integrated computer-aided design and finite element analysis of functionally-graded-material objects", *Materials & Design*, Vol. 28, pp. 2549-65.

Kou, X.Y., Tan, S.T. and Sze, W.S. (2006), "Modeling complex heterogeneous objects with non-manifold heterogeneous cells", *Computer-Aided Design*, Vol. 38, pp. 457-74.

Kumar, V. and Dutta, D. (1998), "Approach to modeling & representation of heterogeneous objects", *Journal of Mechanical Design, Transactions of the ASME*, Vol. 120, pp. 659-67.

Langrana, N.A., Qiu, D., Bossett, E., Danforth, S.C., Jafari, M. and Safari, A. (2000), "Virtual simulation and video microscopy for fused deposition methods", *Materials and Design*, Vol. 21, pp. 75-82.

Liu, H., Maekawa, T., Patrikalakis, N.M., Sachs, E.M. and Cho, W. (2004), "Methods for feature-based design of heterogeneous solids", *Computer-Aided Design*, Vol. 36, p. 1141.

Martin, W. and Cohen, E. (2001), "Representation and extraction of volumetric attributes using trivariate splines: a mathematical framework", *Proceedings of the 6th ACM Symposium on Solid Modeling and Applications*, p. 234.

Musikant, S. (1991), *What Every Engineer Should Know About Ceramics*, M. Dekker, New York, NY.

Nemat-Alla, M. (2003), "Reduction of thermal stresses by developing two-dimensional functionally graded materials", *International Journal of Solids and Structures*, Vol. 40, p. 7339.

Praveen, G.N. and Reddy, J.N. (1998), "Nonlinear transient thermoelastic analysis of functionally graded ceramic-metal plates", *International Journal of Solids and Structures*, Vol. 35, pp. 4457-76.

Qian, X. and Dutta, D. (2003a), "Design of heterogeneous turbine blade", *Computer-Aided Design*, Vol. 35, p. 319.

Qian, X. and Dutta, D. (2003b), "Heterogeneous object modeling through direct face neighborhood alteration", *Computers & Graphics*, Vol. 27, p. 943.

Rossignac, J.R. and Requicha, A.A.G. (1991), "Constructive non-regularized geometry", *Computer-Aided Design*, Vol. 23, pp. 21-32.

Shin, K-H. (2002), "Representation and process planning for layered manufacturing of heterogeneous objects", PhD thesis, University of Michigan, Ann Arbor, MI.

Siu, Y.K. and Tan, S.T. (2002), "Modeling the material grading and structures of heterogeneous objects for layered manufacturing", *Computer-Aided Design*, Vol. 34, p. 705.

Tandon, P. and Kant, A. (2004), "A modelling and manufacturing strategy for the heterogeneous solids", *International Journal of Manufacturing Technology and Management*, Vol. 6, pp. 485-500.

Vijay, C., Swami, M. and Prakash, C.E. (1995), "Voxel-based modeling for layered manufacturing", *IEEE Computer Graphics and Applications*, Vol. 15, pp. 42-7.

Weiler, K. (1988), "The radial-edge structure: a topological representation for non-manifold geometric boundary representations", *Geometric Modelling for CAD Applications, North Holland*, pp. 3-36.

Weiler, K.J. (1986), "Topological structures for geometric modeling", PhD thesis, Rensselaer Polytechnic Institute, Troy, New York, NY.

Weiss, L.E., Merz, R., Prinz, F.B., Neplotnik, G., Padmanabhan, P., Schultz, L. and Ramaswami, K. (1997), "Shape deposition manufacturing of heterogeneous structures", *Journal of Manufacturing Systems*, Vol. 16, pp. 239-48.

Xu, A. and Shaw, L.L. (2005), "Equal distance offset approach to representing and process planning for solid freeform fabrication of functionally graded materials", *Computer-Aided Design*, Vol. 37, pp. 1308-18.

Zhou, M.Y. (2004a), "Adaptive slicing of functionally graded material objects for rapid prototyping", *International Journal of Advanced Manufacturing Technology*, Vol. 24, pp. 345-52.

Zhou, M.Y. (2004b), "Path planning of functionally graded material objects for layered manufacturing", *International Journal of Production Research*, Vol. 42, pp. 405-15.

Zhou, M.Y., Xi, J.T. and Yan, J.Q. (2004), "Modeling and processing of functionally graded materials for rapid prototyping", *Journal of Materials Processing Technology*, Vol. 146, pp. 396-402.

Corresponding author

S.T. Tan can be contacted at: sttan@hku.hk